ISSN 0869-5911, Petrology, 2026, Vol. 34, No. 1, pp. 80–87. © Pleiades Publishing, Ltd., 2026.

Experimental Study of High-Temperature Transformations in Charoitites

A. M. Ionov[a], *, K. A. Gavrilicheva[a], **, O. I. Barkalov[a], A. N. Nekrasov[b], and E. Yu. Dokuchits[c]

[a] *Osipyan Institute of Solid State Physics, Russian Academy of Sciences, Chernogolovka, Moscow oblast, 142432 Russia*

[b] *Institute of Experimental Mineralogy, Russian Academy of Sciences, Chernogolovka, Moscow oblast, 142432 Russia*

[c] *Collaborative Innovation Center for Exploration of Strategic Mineral Resources, China University of Geosciences, Wuhan, China*

**e-mail: ionov@issp.ac.ru*

***e-mail: xenia.gavrilicheva@issp.ac.ru*

Received July 2, 2025; revised August 12, 2025; accepted September 18, 2025

Abstract—This paper reports the investigation of transformations occurring during heating of charoite minerals. Charoite rocks with different color characteristics (lilac, brown, and white asbestiform charoite referred to as charoite-asbestos in the Russian literature) were investigated using mass spectrometry, differential scanning calorimetry and thermogravimetry (DSC–TG), scanning electron microscopy (SEM), *X*-ray diffraction, and Raman spectroscopy. The charoites were heated up to 1200°C. During heating, dehydration and dehydroxylation of lilac, brown, and white charoites were observed in the temperature range 50–500°C. The release of H_2O and OH-groups with an endothermic effect of $\Delta H = 58$ J/g was also detected in white charoite-asbestos at 720–800°C. Our study demonstrated that charoite gradually transforms to wollastonite and, then, to pseudowollastonite at temperatures above 900°C.

Keywords: Murun Massif, charoitite, thermogravimetric analysis, differential scanning calorimetry, mass spectrometry, Raman spectroscopy

DOI: 10.1134/S086959112570033X

INTRODUCTION

The Sirenevyi Kamen deposit of the unique mineral charoite is situated at the boundary of Yakutia and Irkutsk oblast. Murun charoite is a mineral crystallizing together with pyroxenes of the aegirine–diopside–hedenbergite series, richterite–arfvedsonite amphiboles, potassium feldspar, and a number of rare silicate, carbonate (barytocalcite and strontianite), sulfate, and sulfide minerals (Rogova et al., 1978; Vladykin et al., 1983; Konev et al., 1996; Vorob'ev, 2008; Dokuchits et al., 2022).

The genesis of the Murun charoitites has been a matter of debate since their discovery (Rogova et al., 1978; Vladykin et al., 1983, 2016, 2018; Prokofyev and Vorob'ev, 1991; Vladykin and Tsaruk, 2003; Marchuk et al., 2016; Dokuchits et al., 2023). Their magmatic, metasomatic, hydrothermal, and mixed origin was proposed. The first data on the crystallization temperature of charoitites were reported in the 1980s (Rogova, 1980). The homogenization temperatures of fluid inclusions in quartz and tinaksite from charoitites were determined as 350–400°C. According to Prokofyev and Vorob'ev (1991), charoitite formation began at temperatures of 740–565°C and pressures of 4000–650 bar. Biryukov and Berdnikov (1993) supposed that charoitites crystallized at relatively low temperatures of 200–250°C.

Recent investigations of fluid and melt inclusions in the minerals of charoitites (Dokuchits et al., 2025; Vladykin et al., 2018) showed that their formation was related to magmatic and hydrothermal processes, early minerals crystallized at >800°C, and crystallization continued to 600–450°C.

Charoite is a complex silicate of Ca, K, and Na, the composition of which can be described by the general crystal chemical formula $(K,Sr,Ba,Mn)_{15-16}(Ca,Na)_{32}[(Si_{70}(O,OH)_{180})](OH,F)_{4.0}\cdot nH_2O$ (Rozhdestvenskaya et al., 2010). Previous investigations demonstrated that manganese is probably a chromophore in charoites (Nikol'skaya, 1976). Its content is relatively low in white and brown varieties and high in lilac charoite, which was explained by the leaching of K, Na, Ba, Sr, and Mn during weathering and oxidation (Dokuchits et al., 2022).

High-temperature investigations of charoite were reported by Lazebnik et al. (1977), Janeczek (1991), Matesanz et al. (2008), Marchuk et al. (2016), and Ionov et al. (2024); it was found that charoite contains several types of water: tightly bound molecular water, loosely bound molecular water, and weakly bound OH

groups. The most recent experiments of Ionov et al. (2024) showed that water is released from charoite at temperatures of 50–460°C, CO_2 is released at 500–800°C, and the destruction of the mineral structure with charoite to wollastonite transformation occurs at 970–1055°C. Thermograms of charoites of several morphological types (block, plate, long-columnar, and rosette-like) were reported by Lazebnik et al. (1977). However, the high-temperature behavior of charoites of different colors, which probably correspond to different mineral generations, was never studied.

A combined study by various modern experimental methods is required for the better understanding of charoite formation conditions and the determination of the reason of its color variations. We investigated three charoite samples of different colors (lilac, brown, and white charoite-asbestos) at heating up to the melting temperature using the methods of differential scanning calorimetry, thermogravimetry, *X*-ray diffraction, mass spectrometry, and Raman spectroscopy.

METHODS

X-Ray Diffraction

Powder *X*-ray diffraction patterns of the samples were obtained using a Rigaku SmartLAB SE diffractometer equipped with 1D D/TeX PSD in Bragg–Brentano geometry (Cu-$K\alpha_{1,2}$, $\lambda = 1.5418$ Å) at room temperature. The data were collected over a 2θ range of 10°–90° with a step of 0.01°.

Differential Scanning Calorimetry

Charoitite transformations during hearting were investigated on a NETZSCH STA 409 PC/PG apparatus in the mode of simultaneous thermogravimetric, calorimetric, and mass spectrometric analysis up to a temperature of 1200°C. The experiments were conducted at a heating rate of 10.0°C/min in an alundum crucible in an argon atmosphere.

Raman Spectroscopy

Raman spectra were recorded at ambient temperature using a Princeton Instruments HRS-500 spectrometer with a CCD-detector cooled with liquid nitrogen. Raman spectra were excited by a KLM-532 laser with a wavelength of 532 nm. The laser power was ~5 mW on the sample surface. Measurements were conducted in back-scattered geometry. The laser beam was focused to a 3–5 μm spot, and the light scattered by the sample was collected using a 20× Apo Mitutoyo objective lens. In order to obtain Raman spectra above 200 cm^{-1}, the laser line was suppressed using a Semrock edge filter and a TydexNotch-6 holographic filter. The spectral resolution was ~1 cm^{-1} at a grating of 1200 grooves/mm. The absolute accuracy of spectrometer measurement was ±1 cm^{-1} (calibration using spectral lines of a Ne lamp).

CHARACTERISTICS OF INITIAL CHAROITITES

The composition and microstructure of the samples were determined on a Tescan Vega II XMU scanning electron microscope equipped with an INCA Energy 450 energy dispersive spectrometer with an INCA x-sight Si(Li) semiconductor detector and an INCAWave 700 wavelength spectrometer. The investigations were conducted at an accelerating voltage of 20 kV and a beam current of 46.8 nA in an Energy+ mode. Chemical analyses were calculated using the program INCA Suitever.4.15 from the software package The Microanalysis Suite Issue 18d + SP3.

Figure 1 shows back-scattered and secondary electron images of the initial charoitite samples. Charoite occurs in a variety of structural types. Fibrous charoite aggregates often form a fluidal structure around earlier minerals (pyroxene, tinaksite, F-apatite, dalyite, amphibole, and microcline). Lilac charoite contains thin strontianite veinlets, which are visible in back-scattered and secondary electron images (Fig. 1a). Strontianite often occurs in the charoite rocks as an accessory mineral. Brown charoite (Fig. 1b) is fine-grained and has a schistose texture, which envelopes tinaksite grains in the lower part of the sample. A fibrous structure can be seen in the sample of white charoite-asbestos, which shows a slight composition contrast with adjacent wollastonite crystals in back-scattered electron images (Fig. 1c).

The energy dispersive spectrometer was used to determine the contents of Si, Ca, K, Na, Ba, Sr, and Ti, whereas Mn and Fe were analyzed by the wavelength spectrometer. The detection limits at a confidence level of 99.73% were 0.007 wt % for Mn and 0.011 wt % for Fe. The results of the *X*-ray spectral analysis of the samples are given in Table 1.

The chemical compositions of the charoite samples are presented in Table 1. The analysis spots are marked by dots in the BSE images (Fig. 1). The compositions of the three charoite samples are in general similar, which indicates their compositional homogeneity. Rather large wollastonite grains were observed in the white charoite rock (Table 1, area 2, spectra in spots 1, 2, and 6).

Figure 2 shows the *X*-ray diffraction patterns of brown and white charoitites. The results indicate that both samples are dominated by charoite and contain microcline microinclusions. A significant amount of wollastonite was detected in the charoite-asbestos sample.

The Raman spectra of the initial samples (Fig. 3) correspond to the charoite spectra reported by Buzatu and Buzgar (2010). The Raman spectra of lilac

charoite were described in detail previously (Ionov et al., 2024). According to the literature (Richet et al., 1998), three frequency ranges can be distinguished for chain silicates: below 500 cm^{-1} corresponding to metal–oxygen phonon modes, 500–850 cm^{-1} corresponding to the O–Si–O bending vibrations and Si–O_{br} stretching vibrations (O_{br} is bridging oxygen), and 900–1180 cm^{-1} corresponding to the Si–O_{nbr} vibrations (O_{nbr} is nonbridging oxygen). In addition to these ranges, all the spectra contain two high-frequency lines at ~2350 and ~2400 cm^{-1}. These lines are not consistent with the frequency ranges of known phonon modes and are probably of a no-phonon origin. Therefore, it can be supposed that these lines are related to luminescence at a wavelength of ~610 nm.

The Raman spectrum of brown charoite contains peaks not characteristic of the vibrational modes of charoite. The peaks at 1060, 1460, and 1780 cm^{-1} correspond very likely to the vibration modes of carbonate anion CO_3^{2-} (Dufresne et al., 2018). Such spectral features may indicate the presence of carbonate minerals or isomorphic incorporation of CO_3^{2-} in the charoite structure.

The presence of wollastonite inclusions in the charoite-asbestos sample was supported by several independent methods. Elemental analysis (Table 1, white, area 2, wollastonite) revealed a $CaSiO_3$ phase, and *X*-ray structural analysis (Fig. 2b) indicated the presence of a typical wollastonite crystalline structure. Additional supportive evidence was obtained by Raman spectrometry: the spectrum recorded in the second area of the sample (Fig. 3, charoite-asbestos 2) shows distinct main peaks at 410, 635, and 970 cm^{-1} coinciding with the characteristic modes of the reference wollastonite spectrum from the RRUFF database (R040008).

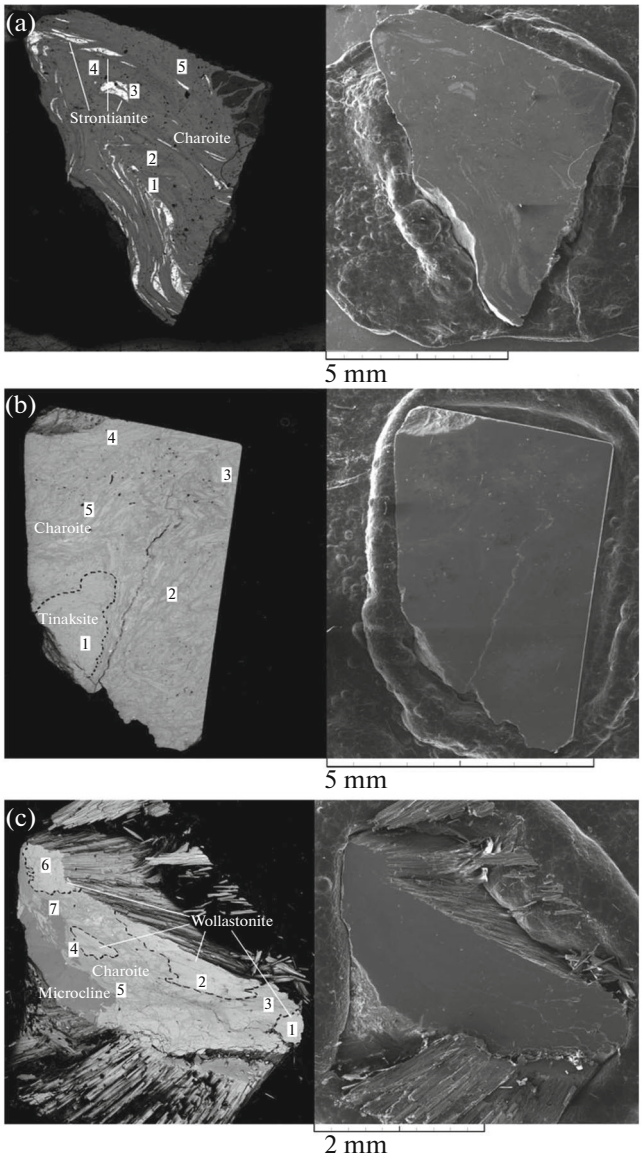

Fig. 1. Back-scattered electron (BSE, left) and secondary electron (SE, right) images of (a) lilac charoite, (b) brown charoite, and (c) charoite-asbestos. The fields of view are 9, 7, and 4 mm, respectively. Numbers indicate the sites of element analysis.

INVESTIGATION OF HIGH-TEMPERATURE TRANSFORMATIONS

The analysis of the results of differential scanning calorimetry and thermogravimetry (DSC–TG) presented in Fig. 4 demonstrated that the charoite samples experienced two stages of mass loss. A rapid loss was observed at temperatures up to 400°C and, then, at approximately 800°C in brown and white charoites only. The TG curve of lilac charoite showed a gradual decrease in sample mass above 400°C. A rapid mass loss (~0.4%) was observed in charoite-asbestos at ~775°C, when an endothermic peak was observed on the DSC curve. The absence of such a peak in the DSC curve of brown charoite could be related to the strong slope of the base line, which prevents the detection of minor thermal effects.

Other features observed on the DSC curves at 950–1000°C are not accompanied by mass losses, and they can be attributed, therefore, to structural transformations, the nature of which has to be elucidated. The high-temperature transformations of lilac charoite were analyzed in detail previously (Ionov et al., 2024).

A comparison of the DSC–TG and mass spectrometric curves of brown and white charoites (Figs. 5a and 5b, respectively) revealed several stages of dehydration and dehydroxylation during heating. Different types of water were released. Charoite contains several types of OH^- groups and H_2O molecules. The first stage up to 200°C corresponds to the release of molecular H_2O loosely bound in the interlayer space of the structure and part of loosely bound hydroxyl groups.

Table 1. Chemical composition of minerals from charoitites; component contents in percent are given at a confidence level of 99.73%

Component	Analytical standard	Lilac	Brown	White	
				area 1, charoite	area 2, wollastonite
SiO_2	SiO_2	60.31 ± 1.66	60.09 ± 1.66	61.43 ± 1.62	50.33 ± 1.53
CaO	Wollastonite	22.39 ± 0.89	22.91 ± 0.90	26.12 ± 0.93	48.20 ± 1.19
K_2O	Orthoclase	10.21 ± 0.56	9.57 ± 0.55	8.69 ± 0.51	<D.L.
Na_2O	Albite	2.12 ± 0.62	2.04 ± 0.61	0.53 ± 0.48	<D.L.
BaO	BaF_2	3.57 ± 0.93	1.86 ± 0.93	1.40 ± 0.78	<D.L.
SrO	SrF_2	<D.L.	0.92 ± 1.34	<D.L.	<D.L.
TiO_2	Ti	<D.L.	2.07 ± 0.53	<D.L.	<D.L.
MnO	Mn	0.250 ± 0.027	0.264 ± 0.029	0.157 ± 0.024	0.380 ± 0.028
FeO	Fe	0.028 ± 0.025	0.175 ± 0.022	0.072 ± 0.023	0.312 ± 0.028

<D.L. indicates below the detection limit.

During the second stage, tightly bound molecular water and hydroxyl groups were released at 200–500°C. The mass spectrometer curves of $m/e = 17$ and 18 of charoite-asbestos (Fig. 5b) show an intense peak at 775°C, which indicates the presence of another water type in the charoite sample.

Lazebnik et al. (1977) investigated the behavior of water in charoites of different morphological types by thermal analysis and IR spectroscopy. They described two stages of water release during charoite heating: elimination of loosely bound water upon heating up to 300°C and the release of residual water at 940–960°C accompanying the destruction of the mineral structure.

According to Vorob'ev (2008), water release from charoite-asbestos begins at 460°C (maximum at 640°C), because it is almost free of loosely bound molecular water and contains only constitutional water. The dehydration temperature increases with decreasing OH^- content (Povarennykh, 1959). Thus, volatile components could be released gradually up to 800°C, and the endothermic effect ($\Delta H = 58$ J/g) at 720–800°C could be related to the loss of constitutional water from charoite-asbestos (Fig. 5b).

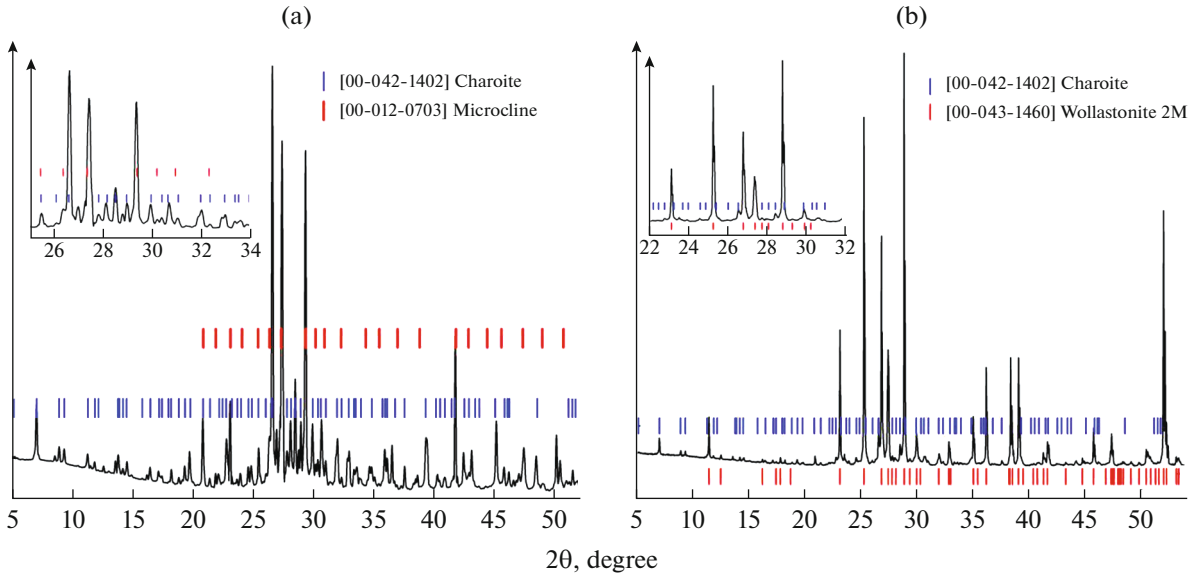

Fig. 2. *X*-ray diffraction patterns (Cu-*Kα* radiation) of the initial samples of (a) brown charoite and (b) charoite-asbestos. Enlarged fragments of the *X*-ray patterns are shown in the insets. Vertical dashes correspond to the diagrams of phases from the ICDD PDF Database.

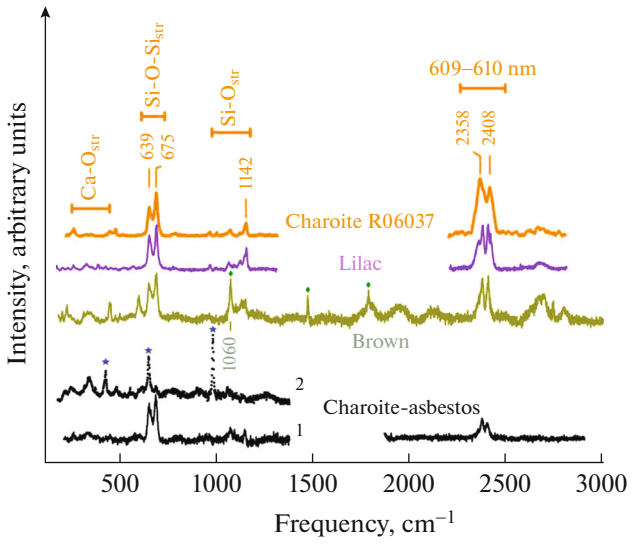

Fig. 3. Raman spectra of the initial charoite samples. From top to bottom: spectrum from the RRUFF database (R06037), lilac charoite, brown charoite, charoite-asbestos (areas 1 and 2). Vertical dashes show the position of peaks, and their frequencies (cm^{-1}) are given above. Horizontal bars are the intervals of vibration frequencies in silicates (Richet et al., 1998).

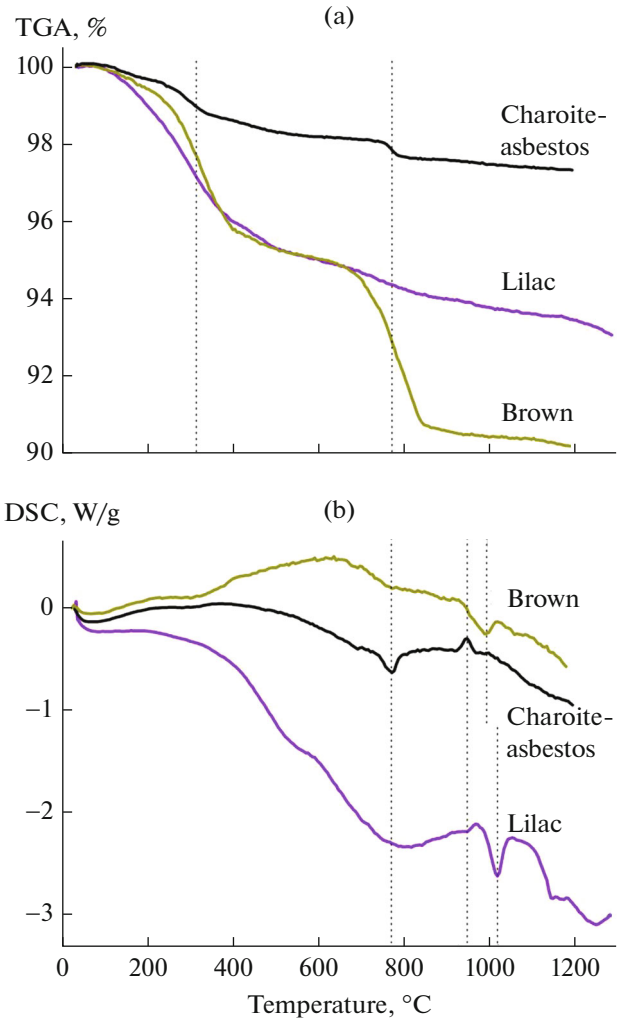

Fig. 4. Curves of (a) TG analysis and (b) DSC over the complete temperature interval for all charoite samples. The heating rate was 10°C/min.

The mass loss of brown charoite at 800°C was related to CO_2 release owing to the decomposition of carbonate groups (Fig. 5a). The appearance of an endothermic peak (ΔH = 53 J/g) at ~1000°C corresponds to charoite transformation to low-temperature wollastonite, which is similar to the transformation of lilac charoite (Ionov et al., 2024). The DSC curve of white charoite-asbestos has specific features. An exothermic peak (ΔH = –18 J/g) was observed at ~950°C. We attributed the observed heat effect to the reaction of wollastonite ($Ca_3Si_3O_9$) formation. It can be supposed that the reaction occurs via heterogeneous nucleation and growth on wollastonite inclusions, which were present in the initial samples. A similar process at the same temperature range was documented by Isaakyan et al. (2020) during wollastonite synthesis.

In order to investigate the minerals by *X*-ray structural analysis and Raman spectroscopy, samples annealed at 1200°C for ~3 h in air were prepared.

The obtained results of *X*-ray analysis and Raman spectroscopy (Figs. 6, 7) demonstrated the transformation of the starting samples to the high-temperature $Ca_3Si_3O_9$ modification pseudowollastonite. Relics of low-temperature wollastonite were also detected in *X*-ray diffraction patterns. The diffraction pattern of brown charoite contains a halo related to partial amorphization during heating.

The Raman spectra of the samples heated up to 1200°C also bear evidence for the presence of pseudowollastonite (Fig. 7). The high-temperature region contains a series of peaks and a rather wide band at 2300–3000 cm^{-1}. A weak peak at ~3350 cm^{-1}, which was obtained in the three samples, coincides with the peak reported by Ionov et al. (2024) for charoite affected by zonal melting and transformation to the high-temperature phase α-$CaSiO_3$. This peak is shifted toward low frequencies relative to the frequency band corresponding to the vibration of hydroxyl groups in charoite (~3550 cm^{-1}). The presence of H_2O and OH^- groups was investigated by IR spectroscopy in charoite by Kaneva et al. (2020) and in the minerals frankamenite (Kaneva et al., 2023) and tinaksite (Kaneva and Shendrik, 2022) associating with charoite. The vibration frequencies of OH^- group are within 3100–3500 cm^{-1}. In these structures, tightly bound OH^- groups are localized on SiO_4 tetrahedra, and the intensity of O–H vibration begins to decrease

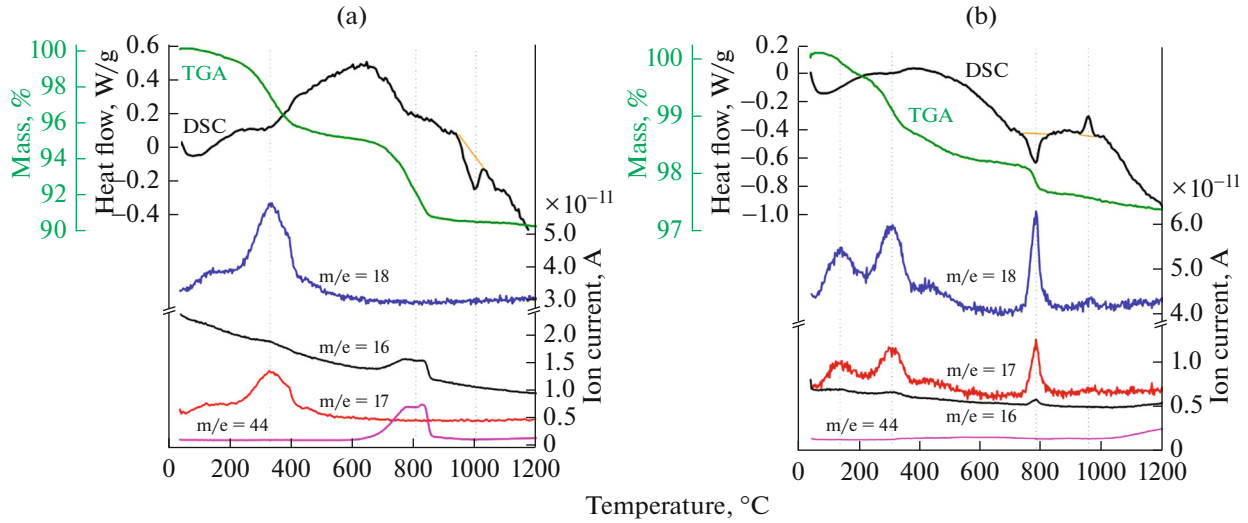

Fig. 5. Mass spectrometric, TG, and DSC curves of (a) brown charoite and (b) charoite-asbestos during heating. The heating rate was 10°C/min.

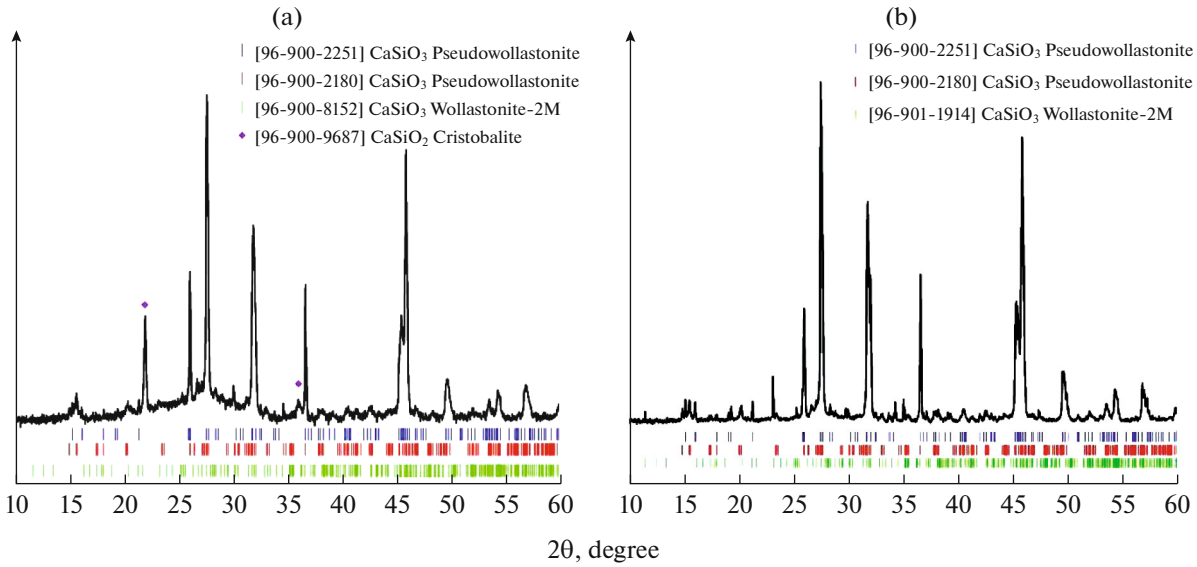

Fig. 6. *X*-ray diffraction patterns of (a) brown charoite and (b) charoite-asbestos annealed at 1200°C in air for 3 h. Vertical dashes below correspond to the diagrams of the major minerals after the Crystallography Open Database.

above 400°C. The accurate interpretation of the ~3350 cm^{-1} band requires further investigations.

Two varieties of white charoite were distinguished in the literature. Vorob'ev (2008) described an early variety of charoite-asbestos with low water and high fluorine contents. Such a charoite variety was found only in calcite carbonatites. The late variety of white charoite was bleached during weathering, and its composition is more similar to brown charoite (low contents of K, Na, Ba, Sr, and Mn). The behavior of charoite-asbestos during heating leaves the question of which type is our sample unanswered. Additional investigations of high-temperature transformations of charoite by the method of in situ X-ray diffraction are planned.

CONCLUSIONS

Three charoite samples from the Murun alkaline–carbonatite massif were studied by mass spectrometry, DSC–TG, *X*-ray diffraction, and Raman spectroscopy.

The DSC–TG curves revealed two stages of mineral dehydration, which resulted in the loss of water bonded in the structure by different mechanisms. The

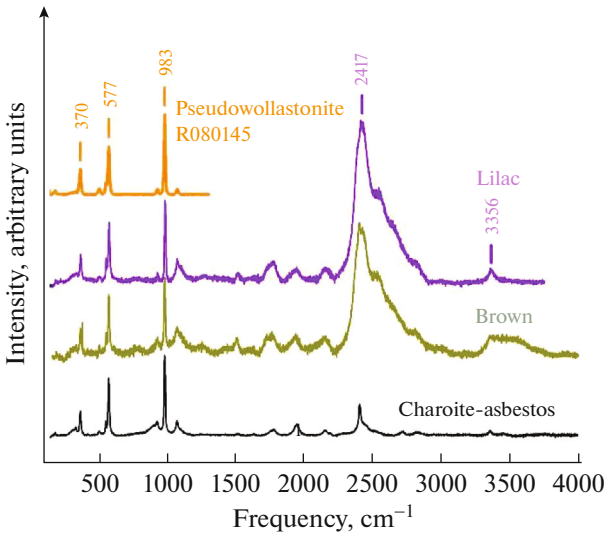

Fig. 7. Raman spectra of charoite annealed in air at 1200°C. From top to bottom: pseudowollastonite spectrum from the RRUFF database (R080145), lilac charoite, brown charoite, and charoite-asbestos. Vertical dashes show the position of peaks, and their frequencies (cm^{-1}) are given above.

heating of charoites released loosely and tightly bound crystallization water up to 500°C, and brown charoite heating to 600–800°C caused the decomposition of the carbonate components of the rock and CO_2 release.

An endothermic peak with ΔH = 53 J/g was recorded in brown charoite above 900°C. It is similar to the peak observed in lilac charoite (Ionov et al., 2024) and related to the charoite–wollastonite transformation. The heating of charoite-asbestos revealed an endothermic peak (ΔH = 58 J/g) at 800°C related to the loss of constitutional water and an exothermic peak (ΔH = –18 J/g) at above 900°C related to the wollastonite-forming reaction. Wollastonite transformation to the high-temperature modification pseudowollastonite began above 1000°C.

ACKNOWLEDGMENTS

The samples were kindly provided by N.V. Vladykin and A.K. Gapeev. The authors are grateful to the Open Analytical Center of the Institute of the Solid State Physics, Russian Academy of Sciences for access to its analytical equipment.

FUNDING

This study was supported by the Ministry of Science and Higher Education of the Russian Federation within the assignment of the Osipyan Institute of Solid State Physics, Russian Academy of Sciences.

CONFLICT OF INTEREST

The authors of this work declare that they have no conflicts of interest.

REFERENCES

Biryukov, V.M. and Berdnikov, N.V., The paragenetic relation between charoite mineralization and alkali metasomatism, *Int. Geol. Rev.*, 1993, vol. 35, no. 7, pp. 585–602.

Buzatu, A. and Buzgar, N., The Raman study of single-chain silicates, *Analele Stiintifice ale Universitatii "Al I Cuza" din Iasi. Seria Geologie*, 2010, vol. 56, pp. 107–125.

Dokuchits, E.Yu., Jiang, S.-Y., Stepanov, A.S., Zhukova, I.A., Radomskaya, T.A., Marfin, A.E., and Vishnevskiy, A.V., Geochemistry of Ca–(K)–(Na) silicates from charoitites in the Sirenevyi Kamen gemstone deposit, Murun Complex, Eastern Siberia, *Ore Geol. Rev.*, 2022, vol. 143, p. 104787. https://doi.org/10.1016/j.oregeorev.2022.104787

Dokuchits, E.Yu., Jiang, S.-Y., Stepanov, A.S., Zhukova, I.A., Radomskaya, T.A., Su, H.-M., and Liu, S.-Q., Mineral associations and in-situ major and trace element compositions of dalyite from charoitites, Murun complex, Siberia, *Ore Geol. Rev.*, 2023, vol. 153, p. 105297. https://doi.org/10.1016/j.oregeorev.2023.105297

Dokuchits, E.Yu., Jiang, S.-Y., Xiong, S.-F., Stepanov, A., Zhukova, I., and Li, W.-T., Fluid and mineral inclusions of charoitite deposit in the Murun alkaline–carbonatite complex, Eastern Siberia, Russia, *J. Geochem. Explor.*, 2025, vol. 274, p. 107735. https://doi.org/10.1016/j.gexplo.2025.107735

Dufresne, W.J.B., Rufledt, C.J., and Marshall, C.P., Raman spectroscopy of the eight natural carbonate minerals of calcite structure, *J. Raman Spectroscop.*, 2018, vol. 49, no. 12, pp. 1999–2007. https://doi.org/10.1002/jrs.5481

Ionov, A.M., Barkalov, O.I., Shulyatev, D.A., and Gavrilicheva, K.A., Experimental studies of charoite mineral transformations under thermal treatment, *Phys. Chem. Mineral*, 2024, vol. 51, pp. 1–7.

Isahakyan, A.R., Zulumyan, N.O., Melikyan, S.A., and Beglaryan, A.A., Synthesis of nanosized β-wollastonite crystals using hydrated silica gel from serpentines, *Russ. J. Pys. Chem. A*, 2020, vol. 94, pp. 2103–2107.

Janeczek, J., Thermal decomposition of charoite, *Mineral. Polonica*, 1991, vol. 22, pp. 21–27.

Kaneva, E. and Shendrik, R., Tinaksite and tokkoite: X-ray powder diffraction, optical, and vibrational properties, *Crystals*, 2022, vol. 12, no. 3, p. 377. https://doi.org/10.3390/cryst12030377

Kaneva, E., Shendrik, R., Pankrushina, E., Dokuchits, E., Radomskaya, T., Pechurin, M., and Ushakov, A., Frankamenite: Relationship between the crystal–chemical and vibrational properties, *Minerals*, 1017, vol. 13, no. 8, p. 1017. https://doi.org/10.3390/min13081017

Kaneva, E.V., Radomskaya, T.A., and Shendrik, R.Yu., *XRF and powder XRD experimental study of charoite: Crystal chemical features of two associated generations, Minerals: Structure, Properties, Methods of Investigation*, Cham: Springer, 2020, pp. 97–104.

Kasatkin, A.V., Cámara, F., Chukanov, N.V., Škoda, R., Nestola, F., Agakhanov, A.A., Belakovskiy, D.I., and Led-

nyov, V.S., Patynite, $NaKCa_4[Si_9O_{23}]$, a new mineral from the Patynskiy Massif, Southern Siberia, Russia, *Minerals*, 2019, vol. 9, no. 10, p. 611.
https://doi.org/10.3390/min9100611

Konev, A.A., Vorob'ev, E.I., and Lazebnik, K.A., *Mineralogiya Murunskogo shchelochnogo massiva* (Mineralogy of the Murun Alkaline Massif), Novosibirsk: SO RAN, NITs OIGGM, 1996.

Lazebnik, K.A., Zayakina, N.V., Lazebnik, Yu.D., and Suknov, V.S., New data on charoite from metasomatic rocks of the Murun massif area, *Mineraly endogennykh obrazovanii Yakutii* (Minerals of Endogenous Formations of Yakutia), 1977, pp. 123–153.

Marchuk, M.V., Medvedev, V., Ya, and Ivanova, I.A., Charoite: Experimental studies, *Geodynam. Tectonophys.*, 2016, vol. 7, pp. 105–118.

Matesanz, E., Garcia-Guinea, J., and Crespo-Feo, E., The high temperature behavior of charoite, *Can. Mineral*, 2008, vol. 46, pp. 1207–1213.

Nikol'skaya, L.V., Novozhilov, A.I., and Samoilovich, M.I., On the nature of coloration of a new alkaline calcium silicate from Eastern Transbaikalia, *Izv. AN SSSR. Ser. geol*, 1976, vol. 10, pp. 116–120.

Povarennykh, A.S., On dehydration and thermal dissociation of minerals, *Tr. Mineral. Muzeya im. Fersmana*, 1959, no. 9, pp. 99–106.

Prokof'ev, Yu.V. and Vorob'ev, E.I., Conditions of formation of strontium-barium carbonatites of the Murunsky alkaline massif of East Siberia, *Geokhimiya magmaticheskikh porod* (Geochemistry of Igneous Rocks), 1991, p. 94.

Richet, P., Mysen, B.O., and Ingrin, J., High-temperature X-ray diffraction and Raman spectroscopy of diopside and pseudowollastonite, *Phys. Chem. Mineral*, 1998, vol. 25, pp. 401–414.

Rogova, V.P., Conditions of formation of charoite rock—a new jewelry and ornamental stone, *Samotsvety. Materialy XI s"ezda MMA*. (Gems. Proceedings of the XI Congress of the MMA.), Nauka, 1980, pp. 79–86.

Rogova, V.P., Rogov, Yu.G., Drits, V.A., and Kuznetsova, N.I., Charoite—a new mineral and a new jewelry and ornamental stone, *Zap. Vsesoyuz. Mineral. O-va*, 1978, vol. 107, no. 1, pp. 94–100.

Rozhdestvenskaya, I.V., Mugnaioli, E., and Czank, M., The structure of charoite, $(K, Sr, Ba, Mn)_{15-16}(Ca, Na)_{32}(Si_{70}(O,OH)_{18}0)_{4.0}\times nH_2O$, solved by conventional and automated electron diffraction, *Mineral. Mag.*, 2010, vol. 74, pp. 159–177.

Vladykin, N.V., Genesis and crystallization of ultramafic alkaline carbonatite magmas of Siberia, ore-potential, mantle sources and relationship with plume activity, *Russ. Geol. Geophys*, 2016, vol. 57, no. 5, pp. 698–712.

Vladykin, N.V. and Tsaruk, I.I., Geology, chemistry, and genesis of Ba-Sr-bearing ("benstonite") carbonatites of the Murun massif, *Russ. Geol. Geophys.*, 2003, vol. 44, no. 4, pp. 325–339.

Vladykin, N.V., Matveeva, L.N., Bogacheva, N.G., and Alekseev, Yu.A., New data on charoite and charoitic rocks, *Mineralogiya i genezis tsvetnykh kamnei Vostochnoi Sibiri* (Mineralogy and Genesis of Colored Stones of Eastern Siberia), Novosibirsk: Nauka, 1983, pp. 41–56.

Vladykin, N.V., Borovikov, A.A., Dokuchits, E.Yu., and Tomas, V.G., Genesis of charoite rocks of the Murun massif, Aldan shield, Russia, *Geochem. Int.*, 2018, vol. 56, no. 12, pp. 1135–1147.

Vorob'ev, E.I., *Charoit (Charoite)*, Novsibirsk: Geo, 2008.

Translated by A. Girnis